

See discussions, stats, and author profiles for this publication at: <https://www.researchgate.net/publication/231523495>

ChemInform Abstract: Polyoxometalates Paneling Through {Mo₂O₂S₂} Coordination: Cation-Directed Conformations and Chemistry of a Supramolecular Hexameric Scaffold.

ARTICLE in JOURNAL OF THE AMERICAN CHEMICAL SOCIETY · JANUARY 2012

Impact Factor: 12.11 · DOI: 10.1021/ja2090383

CITATIONS

17

READS

32

8 AUTHORS, INCLUDING:



Jérôme Marrot

French National Centre for Scientific Research

384 PUBLICATIONS 7,616 CITATIONS

[SEE PROFILE](#)



Sébastien Floquet

Université de Versailles Saint-Quentin

78 PUBLICATIONS 832 CITATIONS

[SEE PROFILE](#)



Xavier López

Universitat Rovira i Virgili

66 PUBLICATIONS 1,589 CITATIONS

[SEE PROFILE](#)



Josep M Poblet

Universitat Rovira i Virgili

243 PUBLICATIONS 5,202 CITATIONS

[SEE PROFILE](#)

Polyoxometalates Paneling through $\{\text{Mo}_2\text{O}_2\text{S}_2\}$ Coordination: Cation-Directed Conformations and Chemistry of a Supramolecular Hexameric Scaffold

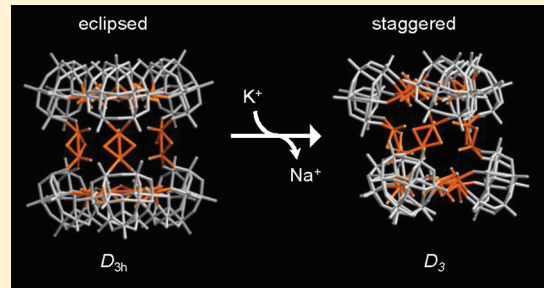
Jérôme Marrot,[†] Marie Anne Pilette,[†] Mohamed Haouas,[†] Sébastien Floquet,[†] Francis Taulelle,[†] Xavier López,[‡] Josep M. Poblet,[‡] and Emmanuel Cadot^{*,†}

[†]Institut Lavoisier de Versailles, UMR 8180, Université de Versailles Saint Quentin, 45 Avenue des Etats-Unis, 78035 Versailles, France

[‡]Departament de Química Física i Inorgànica, Universitat Rovira i Virgili, Marcel·lí Domingo s/n, 43007 Tarragona, Spain

S Supporting Information

ABSTRACT: The chemical system based on the $[\text{Mo}_2\text{O}_2\text{S}_2(\text{OH}_2)_6]^{2+}$ aqua cation (noted L) and the trivacant $[\text{AsW}_9\text{O}_{33}]^{9-}$ polyoxometalate (noted POM) has been investigated. Depending upon the ionic strength and the nature of the alkali cations, these complementary components assemble to yield three different architectures derived as hexamer (**1**), tetramer (**2**), and dimer (**3**). This series of clusters displays the same stoichiometry $\{\text{POM}_6\text{L}_9\}^{36-}$, $\{\text{POM}_4\text{L}_6\}^{24-}$, and $\{\text{POM}_2\text{L}_3\}^{12-}$ for **1**, **2**, and **3**, respectively, and their conditions of formation differ mainly by the nature and the concentration of the alkali cation (from Li to Cs). Structural characterizations of **1** reveal a large hexameric supramolecular scaffold (about 25 Å in diameter), which encloses a large internal hole (about 200 Å³) filled by water molecules and alkali cations (Na⁺ or K⁺). The hexameric scaffold **1** exhibits a rare flexibility property evidenced in the solid state by two distinct conformations, either eclipsed (**1a**) or staggered-off (**1b**). Both conformations appear clearly separated by a large twist angle (~40°) and depend mainly on the composition of the internal hole. Structure of anion **2** shows a tetrahedral arrangement where the four POM units and the six connecting $\{\text{Mo}_2\text{O}_2\text{S}_2\}$ linkers are located at the corners and at the edges, respectively. The structure of anion **3** corresponds to the simplest arrangement, described as a dimeric association of two POM units linked by three $\{\text{Mo}_2\text{S}_2\text{O}_2\}$ pillars. Stability of the hexameric scaffold has been investigated in solution by ¹⁸³W and ³⁹K NMR and by UV-vis, showing that stability of **1** depends strongly on the proportion of potassium ions, which interfere through host-guest exchange. Density functional methodology (DFT) has been applied to compute the geometries and energies of dimer (**3**), tetramer (**2**) and hexamer (**1**) based on $[\text{AsW}_9\text{O}_{33}]$ (POM) and $\{\text{Mo}_2\text{O}_2\text{S}_2\}$ (L) units. Calculations tend to show that internal cations act as “glue” to maintain the POM units connected through the conformationally inward-directed $\{\text{Mo}_2\text{O}_2\text{S}_2\}$ linkers.



INTRODUCTION

The past decade has viewed the development of rational approaches (target-oriented synthesis) toward the generation of sophisticated supramolecular hybrid materials.¹ They result from large organic molecules and inorganic clusters for combining functions and dynamic with varied electronic configuration and bonding patterns within complex structures. The use of the stronger and highly directional metal-ligand interaction has afforded a huge class of materials varying in their sizes, stoichiometries and symmetries, which range from discrete clusters to extended metal-organic framework.² In this sense, the wide structural flexibility of coordination chemistry has made possible to design molecular systems such as rods, grids, rings, tetrahedra, cubes, rotaxanes, and catenanes.³ The hybrid architecture can ensure that interplays between organic and inorganic portions of the molecule originate new phenomena of fundamental and practical interests in the area of catalysis,⁴ molecular recognition,⁵ gas sorption,⁶ medicine,⁷ and memory storage.⁸

In this context, polyoxometalates (POMs) have gained increasing attention, largely due to their unique and unmatched structural disparities,⁹ which result in a wide range of tunable properties such as composition, redox, acidity, electronics, or optics.¹⁰ POMs can include in their molecular framework almost all the elements with various electronic configurations and bonding pattern, which can impart diverse electronic,^{8a,11} magnetic,¹² catalytic,¹³ or other useful properties to molecular-level structures.¹⁴ Striking topological similarities arise between manipulated systems deriving from supramolecular coordination and POMs. Many POM compounds exhibit modular architectures which result generally from the connections of defect (or vacant) subunits to give large macrocycles and super polyhedral arrangements.¹⁵ Diverse strategies can be applied for the POM synthesis, which encompasses a large set of

Received: September 26, 2011

Published: December 13, 2011

parameters and species ranging from the mononuclear metalate species to the bulk oxide. The architectural design principles are almost empirical, mainly based upon the intuition of the synthetic chemist because many successive and interdependent processes and phenomena affect dramatically the overall architecture. The formation of POM species is mainly driven by polycondensation processes of the metalate species which can be drastically altered by different protonation states, the presence of heteroatom templates, heterometallic centers, reducing agents, cations and ligands. Generally, procedures leading to POM-based clusters are simple, consisting of acidifying a solution containing the relevant species listed above. Furthermore, some intensive variables such as ionic strength, pH, temperature and concentration are also of great importance. In short, the formation mechanisms of POMs are still puzzling and are often described by the term "self assembly", not yet well understood in the field of polyoxometalates chemistry. Nevertheless, POM chemistry provides a large set of rigid inorganic ligands useful to develop rich coordination chemistry.¹⁶ These ligand-like polyoxometalates correspond generally to highly negatively charged defect heteropolyoxotungstate ions deriving from Keggin or Dawson saturated ions. Although the geometry and symmetry of the POM ligand and its expected interactions with a metal cation should contain all of the information required for the successful self-assembly, it remains difficult to predict precisely the relevant geometric relationships between the metal coordination sphere and the POM ligand. In aqueous medium, the metallic cations could be involved within polycondensation processes to give polymetallic building blocks with singular coordination requirements,¹⁷ the presence of the silent cations mainly alkali^{18,19} but also organics²⁰ such as organic ammonium cations and in a lesser extent, formation of H-bonds network can also influence the self-assembly process.²¹ Actually, there are few systems, which allow planning the rational and deliberate design and synthesis of POM-based supramolecular clusters. The general choice of POM ligand, metal type and reaction conditions have to be considered in order to restrict the set of fundamental parameters only to those containing the information "programmed" into each component, i.e. the POM ligand and the metallic cation. In other words, the POM ligand should be stable (or metastable) to preclude any structural rearrangements and the reactivity of the metallic cation limited only to the metal–ligand interactions. Thus, the hexaaquo $[M_2O_2S_2(OH_2)_6]^{2+}$ cation ($M = W^V$ or Mo^V) exhibits singular abilities to be used as building block, which clearly differ from those of mononuclear cationic species. While its self-condensation produces remarkable macrocyclic architectures with striking host–guest properties,²² the same $[M_2O_2S_2(OH_2)_6]^{2+}$ unit has been shown to be an efficient ditopic linker for reaction with highly negatively charged heteropolytungstates.²³ The coordination requirements mainly restricted to the equatorial and axial sites of the two equivalent Mo atoms predispose the coordinating groups in a highly predictable way for "edge-on" strategy.

Herein, we report how a simple inorganic system, based on the chemical complementarities between the common trivacant ligand $[B-\alpha-AsW_9O_{33}]^{9-}$ (polyoxometalate unit, noted POM or $\{AsW_9O_{33}\}$) and the ditopic cation $[Mo_2O_2S_2]^{2+}$ (linker unit, noted L or $\{Mo_2\}$) can produce relevant modular assemblies, stereochemically oriented and conformationally ordered through weak supramolecular interactions with alkali cations and water molecules. Depending on the ionic strength and the nature of the alkali cations, three architectures derived as

hexamer (**1**), tetramer (**2**), and dimer (**3**) were isolated and structurally characterized in the solid state. This series of clusters displays the same stoichiometry $\{POM_6L_9\}^{36-}$, $\{POM_4L_6\}^{24-}$, and $\{POM_2L_3\}^{12-}$ for **1**, **2**, and **3**, respectively, and their conditions of formation differ mainly by the nature and the concentration of the alkali cations (from Li to Cs). Surprisingly, the hexameric scaffold (**1**) exhibits a rare flexibility property evidenced by two distinct conformations, either eclipsed (**1a**) or staggered-off (**1b**).

Furthermore, experimental data have been supported by DFT calculations. Geometries and energies of the three assemblies $\{POM_6L_9\}^{36-}$, $\{POM_4L_6\}^{24-}$ and $\{POM_2L_3\}^{12-}$ have been computed to highlight the crucial influence of the cations for the stabilization of the host–guest supramolecular assemblies and for the POM-linker coordination and conformation.

Then, the POM-L based supramolecular self-assemblies appear to be highly versatile and sensitive to the nature of the "chemically" silent cations and represent a powerful chemical tool to develop some challenging POM-based supramolecular engineering concepts toward ionic recognition, dynamic, reversible inclusion of guest, and molecular adaptability.

EXPERIMENTAL SECTION

Physical methods, NMR measurements, X-ray crystallography, computational details, and synthesis of the compounds are given in SI (Supporting Information).

RESULTS AND DISCUSSION

Syntheses. $Na_9[AsW_9O_{33}] \cdot 12H_2O^{24}$ reacts with the aquo dication $[Mo_2O_2S_2(H_2O)_2]^{2+}$ in the ratio 2:3 in aqueous solution at pH = 2. Mixing both reactants provokes a brutal color change from pale yellow to deep red solution, giving an indication of successful $\{POM_xL_y\}$ cluster formation.^{23,25} From this solution, different crude mixed salts (noted $Na_{0.083}K_{5.16}P$, $Na_{1.33}Rb_{4.66}P$ or $Na_{1.08}Cs_{4.91}P$) were isolated through precipitation with good yields between 70 and 90% depending on the source of precipitating agent, i.e. KCl, RbCl or CsCl. These salts have been used as precursors (noted P) for the synthesis of pure crystallized materials, suitable for single crystal X-ray diffraction study or even for direct multinuclear NMR characterizations in solution (^{183}W or ^{39}K). The three precursors exhibit the same $\{AsW_9O_{33}\}/\{Mo_2O_2S_2\}$ stoichiometry and differ in their composition only by the cation content. The infrared spectra of the three salts are nearly the same indicating roughly that the $\{AsW_9O_{33}\}$ subunits retain the same environment in these compounds. As no further characterization has been carried out on these precursors, their formulas have been written with no speculation about their molecular structure and then arbitrarily given for one $\{AsW_9O_{33}\}$ moiety such as $C_xNa_{6-x}[(AsW_9O_{33})(Mo_2O_2S_2)_{1.5}] \cdot nH_2O$ with C = K, Rb or Cs. Depending on the conditions of crystallization, these mixed salts lead selectively to the $\{POM_6L_9\}$, $\{POM_4L_6\}$, and $\{POM_2L_3\}$ anions.

Synthesis of POM_6L_9 Cluster. The hexameric anion $\{POM_6L_9\}$ (noted **1**) is obtained in good yield (30–50%) as pure crystalline materials from solutions of the $Na_{0.083}K_{5.16}P$ crude precursor. Depending on the conditions (pure water, $[NaCl] = 2 \text{ mol} \cdot L^{-1}$ or LiCl from 3 to $10 \text{ mol} \cdot L^{-1}$ solutions), various mixed salts of the $\{POM_6L_9\}$ anion with composition $Na_{1.5}K_{34.5} \cdot \mathbf{1}$, $Na_{32}K_4 \cdot \mathbf{1}$, $Li_{35}K \cdot \mathbf{1}$, and $Li_{25.5}K_{10.5} \cdot \mathbf{1}$ have been obtained, all structurally characterized by X-ray diffraction or ^{183}W NMR.

Synthesis of POM₄L₆ Cluster. At lower ionic strength solutions ($1\text{--}0.7\text{ mol}\cdot\text{L}^{-1}$ LiCl), the $\text{Na}_{1.33}\text{Rb}_{4.66}\text{P}$ or $\text{Na}_{1.08}\text{Cs}_{4.91}\text{P}$ precursors lead selectively to tetrameric arrangements (noted 2) as crystalline materials with good yield (40–50%). Two {POM₄L₆} have been isolated as mixed salts $\text{Cs}_{1.5}\text{Li}_9\cdot2\cdot52\text{H}_2\text{O}$ and $\text{Rb}_{14}\text{Li}_{10}\cdot2\cdot90\text{H}_2\text{O}$, and structurally characterized by X-ray diffraction.

Synthesis of POM₂L₃ Cluster. The dimeric arrangement {POM₃L₂} (noted 3) is obtained from $\text{Na}_{1.08}\text{Cs}_{4.91}\text{P}$ in close conditions that those applied for formation of the tetrameric clusters 2. Crystals of $\text{Cs}_9\text{Li}_3\cdot3\cdot37\text{H}_2\text{O}$ are obtained from 1 $\text{mol}\cdot\text{L}^{-1}$ LiCl solution after heating up to 75 °C. This result shows that conversion relationship exists between the {POM₄L₆} and {POM₂L₃}.

Both are obtained from the same $\text{Na}_{1.08}\text{Cs}_{4.91}\text{P}$ starting precursor, which leads first to the {POM₄L₆} cluster, and then to the {POM₂L₃} anion through moderate heating. The later compound should correspond to the thermodynamic product in such conditions.

From these observations, some rationalizations of the fact that in the solid (crystal structure) and solution, the nature of the alkali cation and their concentration (ionic strength) seem to govern the formation of these three architectures, {POM₆L₉}, {POM₄L₆}, and {POM₂L₃}.

Synthetic observations (depicted in Figure 1) supported by crystal structure analysis and solution studies (presented below) demonstrate that sodium or potassium exhibits intimate interactions with the {POM₆L₉} cage. Therefore, it seems reasonable to assume that these cations direct the self-assembly process toward the formation of the hexameric {POM₆L₉} arrangement and participate directly to its stabilization. Moreover, crystals of 1 are even directly obtained from the $\text{Na}_{0.83}\text{K}_{5.16}\text{P}$ precursor through crystallization procedure using pure water or 2 $\text{mol}\cdot\text{L}^{-1}$ NaCl solution. The compound 1 could be also obtained from various solutions of LiCl giving Li-enriched salts $\text{K}_{25.5}\text{Li}_{10.5}\text{-1}$ and $\text{KLi}_{35}\text{-1}$, which exhibit high solubility in water for ^{183}W and ^{39}K NMR studies.

The behaviors of the $\text{Na}_{1.33}\text{Rb}_{4.66}\text{P}$ and $\text{Na}_{1.08}\text{Cs}_{4.91}\text{P}$ precursors are quite different. Attempts of their recrystallization in pure water did not succeed, mainly due to the low solubility of these salts in this medium. On the other hand, crystallizations in 1 $\text{mol}\cdot\text{L}^{-1}$ LiCl solutions were however successful

at growing crystals corresponding to the tetrameric {POM₄L₆} arrangement. This information indicates that bigger cations such as Rb⁺ or Cs⁺ associated to a low content in Na⁺ cation and moderate concentrations in Li⁺ show a weak ability to maintain the {POM₆L₉} arrangement.

Structure of the Anions. Crystal data of $\text{K}_{3.5}\text{Na}_{32.5}\text{-1a}\cdot120\text{H}_2\text{O}$, $\text{KLi}_{35}\text{-1a}\cdot196\text{H}_2\text{O}$, $\text{K}_{34.5}\text{Na}_{1.5}\text{-1b}\cdot90\text{H}_2\text{O}$, $\text{Rb}_{14}\text{Li}_{10}\cdot2\cdot90\text{H}_2\text{O}$, $\text{Cs}_{15}\text{Li}_9\cdot2\cdot52\text{H}_2\text{O}$ and $\text{Cs}_9\text{Li}_3\cdot3\cdot37\text{H}_2\text{O}$ are given in Table S1 (see Supporting Information).

$\text{K}_{3.5}\text{Na}_{32.5}[\text{AsW}_9\text{O}_{33}]_6[\text{Mo}_2\text{O}_2\text{S}_2]_9\cdot120\text{H}_2\text{O}$, $\text{K}_{3.5}\text{Na}_{32.5}\text{-1a}\cdot120\text{H}_2\text{O}$. The polyhedral representation of {POM₆L₉} 1a is shown in Figure 2. Structure of 1a reveals a large scaffolding arrangement where covalent interactions between the POM units and the {Mo₂O₂S₂} linkers result in a single mode of connections. Each Mo atom is coordinated to two adjacent oxygen atoms belonging to the {AsW₉O₃₃} subunit. The supermolecular hexamodular anion {POM₆L₉} can be described as two basal triangular subunits {POM₃L₃} (see Figure 2a) mutually connected by three additional {Mo₂O₂S₂} linkers, which act as pillars within the scaffold structure. Both triangular units appear nearly superimposed, giving an eclipsed conformation for the cluster 1a, properly described with the idealized D_{3h} symmetry. The nine {Mo₂O₂S₂} linkers point their axial Mo=O bonds toward the inner cage of the cluster and all the molybdenum atoms display the usual distorted square-pyramidal environment.^{23,25} The bond lengths within {AsW₉O₃₃}⁹⁻ subunits and {Mo₂O₂S₂}²⁺ linkers are usual and correspond to those commonly observed in similar compounds.²⁶ The Mo–O–W connecting bridges display also the expected bond lengths, longer for the Mo–O bonds [1.94(2)–2.01(2) Å] and significantly shorter for the W–O bonds [1.78(2)–1.84(2) Å]. As a consequence of the geometrical arrangement, the angles of Mo–O–W bridges belonging to the both triangular basal units appear larger [149(1)–155(1) $^\circ$] than those involving the {Mo₂O₂S₂} pillars [137(1)–142(1) $^\circ$]. The hexagonal paneling of the six {AsW₉O₃₃} subunits through the {Mo₂O₂S₂} coordination delimits a large hydrophilic hole lined by the eighteen inner terminal oxygen atoms of the nine {Mo₂O₂S₂} groups. The large inner volume (about 200 Å³) is filled by six sodium cations which form two embedded and

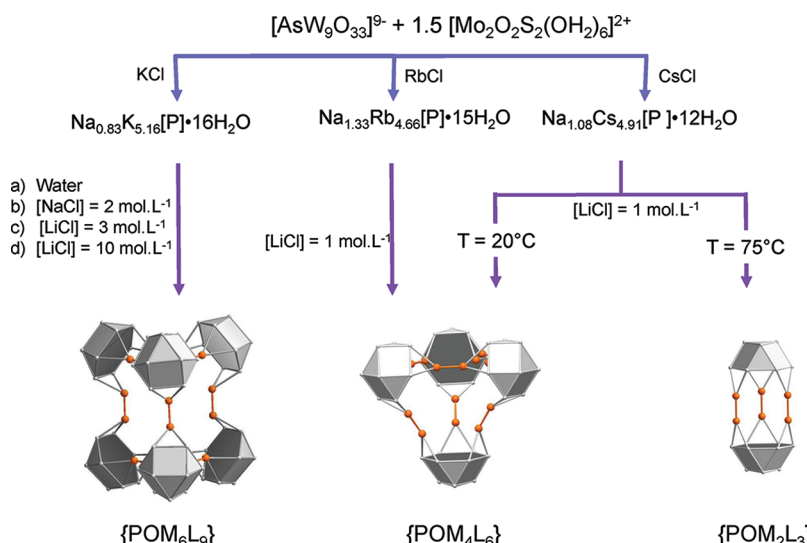


Figure 1. Schematic view of the conditions of formation of the polymodular anions {POM_nL_{1.5n}} with $n = 6, 4$, or 2 ; POM = {AsW₉O₃₃} and L = {Mo₂O₂S₂}.

The three arrangements are obtained from a common precursor (noted P) through crystallization processes differing by ionic strength, nature of the counterion or temperature.

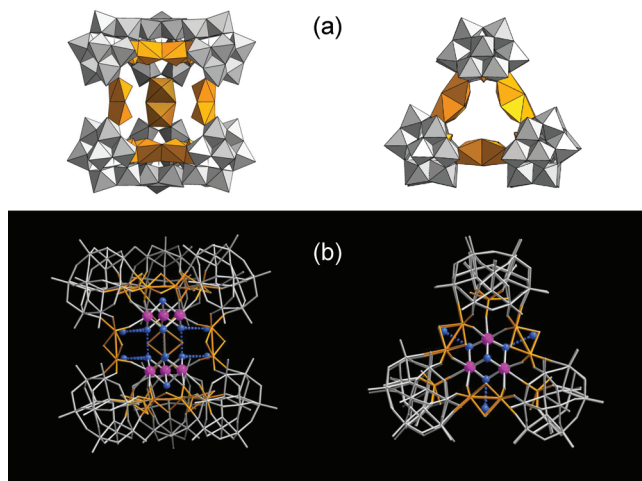


Figure 2. Structural views of the eclipsed conformation of $\{\text{POM}_6\text{L}_9\}$ scaffold (anion **1a**). (a) Polyhedral representations showing the connections between both triangular basal units through three $\{\text{Mo}_2\text{O}_2\text{S}_2\}$ pillars (left) and highlighting the eclipsed arrangement of the two triangular basal units $\{\text{POM}_3\text{L}_3\}$ (right); (b) Mixed wire/stick representations showing the inner cationic cluster $\{\text{Na}_6(\text{H}_2\text{O})_{14}\}^{6+}$ which consists of two stacked triads $\{\text{Na}_3(\text{OH}_2)_7\}^{3+}$. Color codes: Gray polyhedra or wires = $\{\text{AsW}_9\text{O}_{33}\}$ unit, orange polyhedra or wires = $\{\text{Mo}_2\text{O}_2\text{S}_2\}$, linker L; pink spheres = sodium cations; blue spheres = water molecules. Dashed blue lines = O...O interactions through hydrogen bonds.

stacked $\{\text{Na}_3(\mu_2\text{-OH}_2)_3(\mu_3\text{-OH}_2)\}^{3+}$ triads (see Figure 2b). The Na^+ cations considered as equivalent in the D_{3h} idealized symmetry exhibit octahedral environments with the expected $\text{Na}-\text{O}$ bond lengths which fall in a narrow range (2.30 ± 0.05 Å). Octahedra connections within the triads are face-shared, ensured by the μ_2 - and $\mu_3\text{-OH}_2$ attached water molecules. The coordination sphere of each sodium cation is completed by three vicinal terminal oxygen atoms belonging to three $\{\text{Mo}_2\text{O}_2\text{S}_2\}$ linkers which thus anchor both $\{\text{Na}_3\mu_2\text{-OH}_2\}_3(\mu_3\text{-OH}_2)\}^{3+}$ clusters to the polyoxothiomolybdate inner cavity. The $\text{Na}-\text{O}$ bond distances within the six $\{\text{NaO}_3(\text{OH}_2)_3\}$ inner octahedra fall in the expected range [2.21(2)–2.40(3) Å]. Furthermore, six additional water molecules are located at the apertures of the cavity, distributed as three pairs between the $\{\text{Mo}_2\text{O}_2\text{S}_2\}$ pillars. These water molecules interact weakly through H-bonds with the $\mu_2\text{-OH}_2$ of the triads [2.69(3)–2.80(3) Å]. Besides, the two $\{\text{Na}_3\}$ clusters surrounded by their three solvating water molecules are stacked up within the cavity, interacting together through six parallel H-bonds [2.60(4)–2.87(4) Å] (see Figure 2b). In summary, the D_{3h} hexameric cavity encloses six sodium cations and fourteen water molecules, arranged in a supramolecular cluster.

KLi₃₅[{AsW₉O₃₃}₆(Mo₂O₂S₂)₉]2O, KLi₃₅·**200H₂O.** The structure of KLi₃₅**·**1a2O reveals an hexameric $\{\text{POM}_6\text{L}_9\}$ arrangement, similar to that previously observed in K_{3.5}Na_{32.5}**·**1a2O (see Figure 2). Likewise, the inner cavity contains fourteen water molecules which occupy very close positions of those observed within K_{3.5}Na_{32.5}**·**1a2O. Weak electronic densities were found at the centers of the six octaedral sites defined by three water molecules and three terminal oxo groups belonging to the linkers and refined with lithium. The resulting Li–O bond distances are usual for Li cations in octaedral environment (Li–O = 2.08(1)–2.24(3) Å).²⁷ These distances are significantly shorter than those observed for $\{\text{NaO}_6\}$ octahedra that results in a

contraction of the two stacked $\{\text{Li}_3(\mu_3\text{-OH}_2)(\mu_2\text{-OH}_2)_3\}^{3+}$ aqua cationic clusters, thus reducing the distances between the water molecules within each triad from 3.38 ± 0.04 Å with Na^+ to 3.08 ± 0.07 Å with Li^+ . Conversely, the intertriad separation (corresponding to the separation between the mean planes defined by the three M⁺ cations of the two triad $\{\text{M}_3\}$) increases significantly from 5.4 to 6.0 Å for M = Na and M = Li, respectively. As a consequence, none intertriads interactions through hydrogen bonds are observed since the O...O distances increase from ~2.8 to 3.4 Å. Furthermore, the elemental analysis of the compound KLi₃₅**·**1a2O reveals the presence of one single potassium cation which has not been located in the structure, because it should be severely disordered with water molecule as external counterion.

K_{34.5}Na_{1.5}[{AsW₉O₃₃}₆(Mo₂O₂S₂(H₂O))₆(Mo₂O₂S₂)₃]2O, K_{34.5}Na_{1.5}·**1b2O.** The structure of the $\{\text{POM}_6\text{L}_9\}$ anion **1b** is depicted in Figure 3. The arrangement in **1b** derives

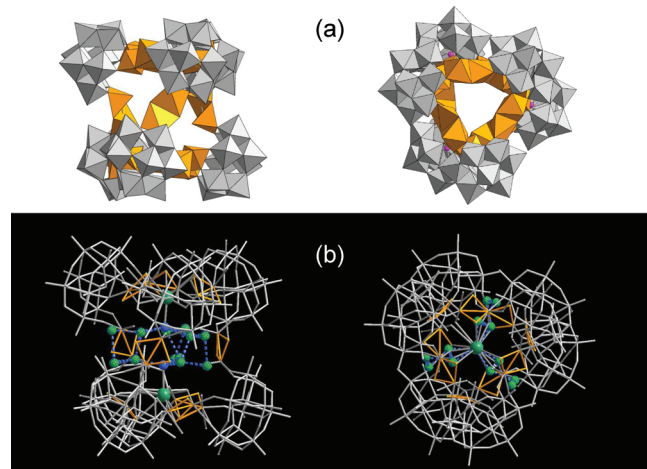


Figure 3. Structural views of the staggered conformation of $\{\text{POM}_6\text{L}_9\}$ scaffold (anion **1b**). (a) Polyhedral representations showing the screwed distortions between both triangular basal units (left) and highlighting the resulting 40° staggered conformation (top view, right). (b) Mixed wire/stick representations showing the $\{\text{K}_8(\text{OH}_2)_8\}^{8+}$ embedded cluster composed by two apical crypted potassium atoms and twelve inner K/OH₂ mixed sites. Color codes: Gray polyhedra or wires = $\{\text{AsW}_9\text{O}_{33}\}$ unit, orange polyhedra or wires = $\{\text{Mo}_2\text{O}_2\text{S}_2\}$, linker L; pink, green, blue and mixed green-blue spheres = arsenic atoms, potassium cations, water molecules and disordered potassium cations/water molecules sites, respectively. Dashed blue lines = O...O or K...O interactions.

topologically from the hexameric anion **1a** described above. Nevertheless, the striking feature for **1b** lies in its pronounced conformational change. In **1b**, the hexameric scaffold appears strongly distorted to decrease the nominal symmetry from D_{3h} to D_3 (see Figure 3a). The anion **1b** is chiral (D_3 symmetry), but the crystal is a racemic mixture of clusters ($P12_1/n$, centrosymmetric space group). In such an arrangement, both triangular basal units adopt a pronounced staggered conformation of about 40°. The screwed torsion of the $\{\text{POM}_6\text{L}_9\}$ scaffold from eclipsed conformation observed in **1a** to strongly staggered in **1b** highlights the high flexibility of the hexameric skeleton, rarely observed in polyoxometalate structures. Then, flexibility does not occur from the $\{\text{AsW}_9\text{O}_{33}\}$ POM units, which exhibit the usual rigid metal–oxygen close packing, but, in this case, arises from the $\{\text{Mo}_2\text{O}_2\text{S}_2\}$ linkers able to distort their coordination polyhedra. It is worth noting that the Mo atoms

of the linkers belonging to the triangular basal units display distinct coordination numbers. One Mo atom retains a square pyramidal environment while the other is coordinated to an outer water molecule (identified by a longer Mo–O bond length ranging between 2.54(2) and 2.64(2) Å) and exhibits an octahedral geometry. On the other hand, the square-pyramidal geometry is retained for the Mo centers of three $\{\text{Mo}_2\text{O}_2\text{S}_2\}$ pillars. The magnitude of the distortion can be evaluated through examination of relevant geometrical parameters such as torsion angles between vertexes defined by the double sulphido bridge of the $\{\text{Mo}_2\text{O}_2\text{S}_2\}$ and the two equatorial oxo groups ensuring the W–O–Mo junctions. These angles are quite closed for the octahedral Mo center (about 2°) but significantly larger for the square pyramidal Mo centers (between 16° and 24°). As a consequence of the staggered conformation, the two triangular basal units appear slightly distorted, resulting from a slight tilting of the three $\{\text{AsW}_9\text{O}_{33}\}$ moieties (see Figure 4).

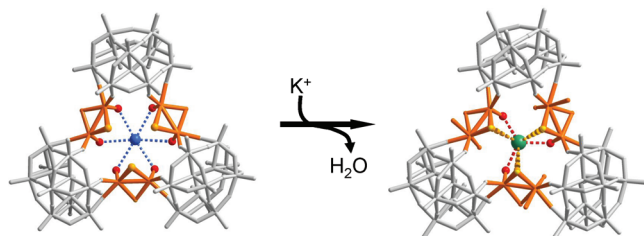


Figure 4. Size adaptability of the apical sites within the $\{\text{POM}_6\text{L}_9\}$ scaffold. Formal substitution of a water molecule (blue sphere) for a potassium cation (green sphere) leads to a size reduction of the $\{\text{POM}_3\text{L}_3\}$ apical site through a concerted compulsion of the overall scaffold.

From these geometrical observations, the $\{\text{Mo}_2\text{O}_2\text{S}_2\}$ linkers can be considered as flexible hinges, allowing a concerted screwed torsion of the anionic scaffold. Within the cavity, two apical potassium cations were unambiguously found along the C_3 axis and located at the center of both distorted triangular basal units (see Figure 3b). These K^+ ions are 7-fold coordinated with three terminal oxo groups ($\text{K}-\text{O} \approx 2.69$ Å) and three sulfur atoms ($\text{K}-\text{S} \approx 3.35$ Å) belonging to the $\{\text{Mo}_2\text{O}_2\text{S}_2\}$ linkers and with a single inner water molecule, located at the central C_3 axis ($\text{K}-\text{OH}_2 \approx 2.74$ Å). Furthermore, ambiguous electronic density was found on twelve inner sites, distributed as three groups of four sites related by the C_3 operation (in the D_3 approximation). These positions can be refined satisfactory with 50% oxygen atoms (water molecules) statistically disordered with 50% potassium atoms, leading to six supplementary embedded potassium cations (see Figure 3b). These potassium atoms can be statistically distributed as two pairs over each set of four sites leading to consistent $\text{K}\cdots\text{K}$ separations (~3.4–3.5 Å) and giving 6-fold coordinated potassium cations surrounded by water molecules or terminal oxo groups ($\text{K}-\text{O} = 2.5$ –3.2 Å). Such a structural analysis implies the presence of eight embedded positive charges arranged as a large $\{\text{K}_8(\text{OH}_2)_8\}^{8+}$ guest aquo cluster. Several arguments support the structural analysis of the embedded cationic cluster. The main one is based upon the presence of cationic charges crucial for the stability of the highly negatively charged $\{\text{POM}_6\text{L}_9\}^{36-}$ backbone. Six Na^+ or Li^+ cations were found in the eclipsed $\{\text{POM}_6\text{L}_9\}$ structure **1a**. It should be consistent to find a comparable number of cations in the staggered conformation **1b**. DFT calculations reported below

show that structure optimizations of the $\{\text{POM}_6\text{L}_9\}$ scaffold **1a** required the presence of positive charges, crucial to keep the connection between the six $\{\text{AsW}_9\text{O}_{33}\}^{9-}$ POM units. Furthermore, these DFT results demonstrate even that the presence of the six guest sodium cations is not sufficient to optimize properly geometric parameters of the hexamer and additional sodium cations, located outside the cavity are required to give consistency between experimental and theoretical DFT calculations. The other argument is based on the observed distortions, which lead to the pronounced staggered conformation for **1b** and its related driving force. In **1b**, only sixteen atoms were found inside the cluster while **1a** contains twenty atoms distributed as fourteen water molecules and six Na^+ or Li^+ cations. It becomes intuitive that this distortion could be attributed to the compulsion of the system to minimize the empty volume of the cavity. Such a constraint must be reinforced by the presence of potassium ions distributed over these fourteen sites, which results in a decrease of the interatomic distances and in stronger attractive electrostatic interactions between the flexible $\{\text{POM}_6\text{L}_9\}$ host and the inner cationic guest cluster. Obviously, it becomes evident that the conformational change of the hexameric cluster arises from a cooperative effect that involves interactions between the overall cationic guest and the eighteen internal terminal oxo groups of the nine $\{\text{Mo}_2\text{O}_2\text{S}_2\}$ linkers. Therefore, the host–guest adaptability of the system is clearly illustrated by the water/potassium substitution at the two apical sites, located at the center of the two triangular basal units $\{\text{POM}_3\text{L}_3\}$ (see Figure 4). In **1a**, each apical water molecule interacts smoothly through H-bonds with the six surrounding oxo groups with the usual $\text{O}\cdots\text{O}$ distances [3.12(2)–3.18(2) Å]. In **1b**, upon the distortion of the cluster, the size of both apical site is reduced to give three short $\text{K}-\text{O}$ and three $\text{K}-\text{S}$ contacts [2.68(2)–2.70(2) Å] and [3.31(2)–3.39(2) Å], respectively and fits preferentially with the coordination sphere of the potassium ion.

$\text{Rb}_{14}\text{Li}_{10}[(\text{AsW}_9\text{O}_{33})_4(\text{Mo}_2\text{O}_2\text{S}_2(\text{H}_2\text{O}))_6]\cdot 90\text{H}_2\text{O}$ (**Rb₁₄Li₁₀·2**). Anion **2** consists of a tetrahedral “edge-on” arrangement, where the four $\{\text{AsW}_9\text{O}_{33}\}$ POM units constitute the corners and the six $\{\text{Mo}_2\text{O}_2\text{S}_2\}$ linkers located on the vertexes (see Figure 5).

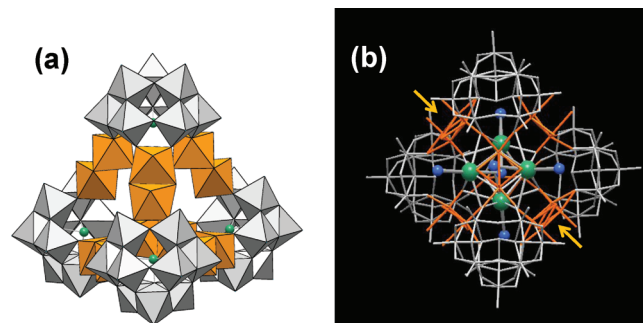


Figure 5. Structural views of the tetrahedral $\{\text{POM}_4\text{L}_6\}$ self-assembly (anion **2**). (a) Polyhedral representation. (b) Mixed wires/ball-and-stick representation highlighting the two disordered $\{\text{Mo}_2\text{O}_2\text{S}_2(\text{H}_2\text{O})_2\}$ linkers (marked by arrows) associated to disordered Rb^+ cations distributed over the four facial sites. Color codes: gray wires = $\{\text{AsW}_9\text{O}_{33}\}$ subunits; orange wires = $\{\text{Mo}_2\text{O}_2\text{S}_2(\text{H}_2\text{O})_2\}$ linkers; green sphere = Rb^+ cations; blue spheres = water molecules.

The four faces of the tetrahedral arrangement consisting of four regular (undistorted) triangular basal units with similar modes

of connection between $\{\text{Mo}_2\text{O}_2\text{S}_2\}$ linkers and $\{\text{AsW}_9\text{O}_{33}\}$ moieties that those previously observed in **1a** and **1b** anions. All twelve molybdenum display an attached terminal aquo ligand in their coordination sphere to give an octahedral environment for each of them [$\text{Mo}-\text{OH}_2 \approx 2.50(2)$ Å]. Two opposite $\{\text{Mo}_2\text{O}_2\text{S}_2\}$ linkers exhibit a structural disorder, which consists of the splitting of the involved Mo atoms over two close positions separated by about $0.90(1)-1.00(1)$ Å (shown in Figure 5b). One disordered linker is consistent with occupancy factors of 0.3 and 0.7 for the split Mo atoms while the other leads to equal 0.5 occupancy factors over the two Mo positions. Such local disorders are frequently observed in similar arrangements, and are explained properly by the statistical 180° reversal of the concerned $\{\text{Mo}_2\text{O}_2\text{S}_2(\text{OH}_2)_2\}$ groups, then subsequently pointing their $\text{Mo}=\text{O}$ terminal bonds (and alternately, their $\text{Mo}-\text{OH}_2$ groups) either inward or outward the anion.²⁸ Furthermore, such positional disorders should be probably correlated with the distribution of the enclosed rubidium cations, found disordered at the centers of the four triangular basal units of the supertetrahedron (see Figure 5b). Each Rb^+ cation interacts with six terminal oxygen ($\text{Rb}-\text{O} = 3.21(2)$ Å) and three bridging sulfur atoms ($\text{Rb}-\text{S} = 3.60(1)$ Å), belonging to three adjacent $\{\text{Mo}_2\text{O}_2\text{S}_2\}$ linkers. These rubidium atoms are bound to an external water molecule and are mutually bridged by an additional inner water molecule (Figure 5b). In such an arrangement, the $\text{Rb}-\text{O}$ and $\text{Rb}-\text{S}$ bond distances are very close to the sum of van der Waals radii (~ 3.0 and ~ 3.45 Å for $\text{Rb}-\text{O}$ and $\text{Rb}-\text{S}$, respectively), thus indicating that the size of the regular sites matches sterically with that of the Rb^+ cation. The observed disorder which involves the Mo atoms of two linkers and Rb^+ cations could result from several superimposed arrangements noted $\{\text{POM}_{4,4}\text{L}'_x\}$ with $x = 0, 1$, or 2, differing in the number of 180° reversed $\{\text{Mo}_2\text{O}_2\text{S}_2(\text{OH}_2)_2\}$ groups (noted L'). Each arrangement should enclose a specific number of Rb^+ cations, related to the distribution between inward and outward $\text{Mo}=\text{O}$ bonds. DFT calculations (see below) clearly demonstrate that the anionic character of the cavity (correlated with the presence of inner cations) is mainly due to the presence of inward terminal oxo groups. The tetrameric arrangement has been also structurally characterized as a cesium salt. $\text{Cs}_5\text{Li}_9\text{-}2$ is isostructural to $\text{Rb}_{14}\text{Li}_{10}\text{-}2$ and exhibits similar molecular arrangement and related intrinsic disorder.

$\text{Cs}_9\text{Li}_3[(\text{AsW}_9\text{O}_{33})_2(\text{Mo}_2\text{O}_2\text{S}_2)_3]\cdot 33\text{H}_2\text{O}$ ($\text{Cs}_9\text{Li}_3\text{-}3\cdot 33\text{H}_2\text{O}$).

The arrangement of **3** corresponds to the simplest topology able to be produced by the $\{\text{AsW}_9\text{O}_{33}\}$ - $\{\text{Mo}_2\text{O}_2\text{S}_2\}$ system (Figure 6). **3** corresponds to a dimodular anion $\{\text{POM}_2\text{L}_3\}$, resulting from the connections of three $\{\text{Mo}_2\text{O}_2\text{S}_2\}$ linkers arranged as parallel pillars between two chelating $\{\text{AsW}_9\text{O}_{33}\}$ moieties (D_{3h} idealized symmetry). Due to steric hindrance, all six molybdenum atoms exhibit a square pyramidal geometry with outward-directed $\{\text{Mo}=\text{O}\}$ groups. It should be noted that a similar topology was already found in the $[(\text{PW}_9\text{O}_{34})_2(\text{Mo}_2\text{O}_2\text{S}_2(\text{OH}_2)_2)_3]^{12-}$ anion.^{28a} However, the nature of the isomerism of the trivacant precursor, A-type in $[\alpha\text{-}\text{PW}_9\text{O}_{34}]^{9-}$ and B-type in the $[\alpha\text{-AsW}_9\text{O}_{33}]^{9-}$ subunit gives rise to two distinct situations mainly governed by steric constraints. In the B-type isomerism, the reduced $\{\text{O}_6\}$ perimeter defined by the six chelating oxo groups within the $[\text{AsW}_9\text{O}_{33}]^{9-}$ subunit leads to a close-compact arrangement for the three $\{\text{Mo}_2\text{O}_2\text{S}_2\}$ pillars ($S\cdots S$ van der Waals contacts of 3.56 Å).

Solution ^{183}W and ^{39}K NMR Studies of $\{\text{POM}_6\text{L}_9\}$

Cluster. The high solubility of the $\text{K}_{3,5}\text{Na}_{32,5}\text{-}1\text{a}$ and $\text{KLi}_{35}\text{-}1\text{b}$ in $\text{D}_2\text{O}-\text{H}_2\text{O}$ allowed recording ^{183}W NMR spectra with a good

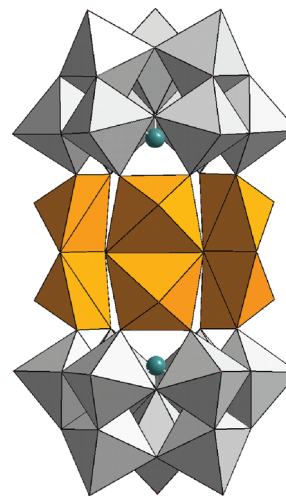


Figure 6. Polyhedral view of the dimeric $\{\text{POM}_2\text{L}_3\}$ arrangement (anion **3**). Gray and orange polyhedra = $\{\text{AsW}_9\text{O}_{33}\}$ and $\{\text{Mo}_2\text{O}_2\text{S}_2\}$ linkers, respectively.

signal/noise ratio from direct dissolution of the structurally characterized crystalline materials (Figure 7a and 8a, respectively). The ^{183}W NMR spectrum of $\text{K}_{3,5}\text{Na}_{32,5}\text{-}1\text{a}$ exhibits five well-resolved and sharp resonances with intensity ratio 2:2:2:1:2 (Figure 7a) corresponding to the nine tungsten atoms involved

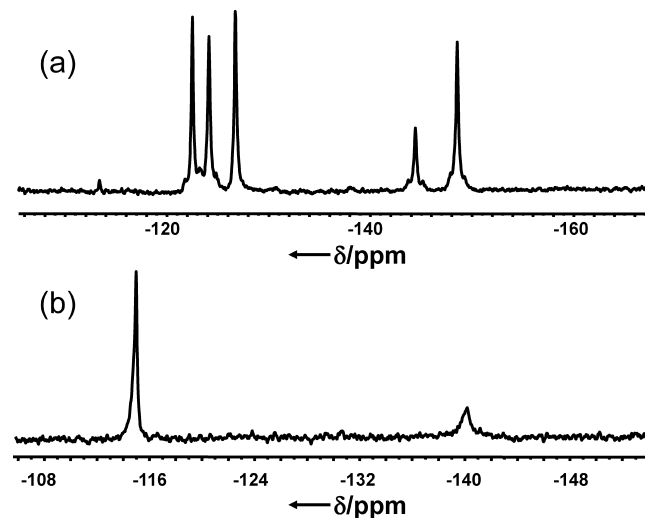


Figure 7. ^{183}W NMR spectra of (a) $\text{K}_{3,5}\text{Na}_{32,5}\text{-}1\text{a}$ showing five well-resolved lines consistent with the hexameric $\{\text{POM}_6\text{L}_9\}$ scaffold and (b) pure lithium salts of **1** or **3** obtained through ion-exchange process exhibiting two resonances in accordance with the dimeric species $\{\text{POM}_2\text{L}_3\}$.

within the six equivalent $\{\text{AsW}_9\text{O}_{33}\}$ subunits exhibiting a C_s local symmetry. Such a distribution is consistent with the solid-state structure of **1a** and attests to the fair stability of the $\{\text{POM}_6\text{L}_9\}$ as a mixed K–Na salt over the acquisition period (~ 18 h). In addition, the chemical shifts spreading from -120 to -150 ppm correspond to the expected values for W^{VI} atoms in an octahedral oxo environment.²⁹ Conversely, the $\text{KLi}_{35}\text{-}1$ salt exhibits a distinct behavior in solution (see Figure 8a), featured by a strongly time dependent ^{183}W NMR spectrum. The $\text{KLi}_{35}\text{-}1$ sample was concentrated enough (about 0.1 mol·L $^{-1}$) to carry out ^{183}W NMR kinetic experiments. Each ^{183}W NMR spectrum was acquired for 2 h over an 88 h total

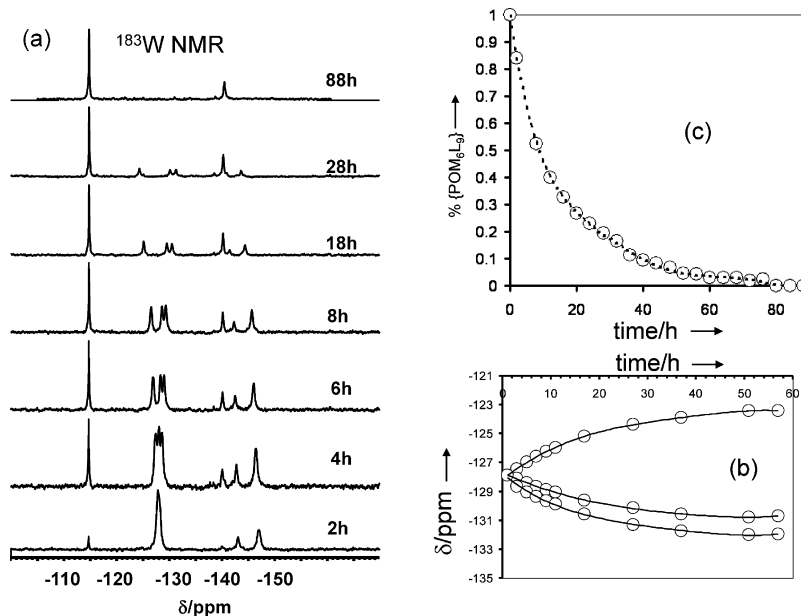


Figure 8. (a) Selected ¹⁸³W NMR spectra of KLi₃₅-1a highlighting the slow conversion of the hexameric {POM₆L₉} scaffold at 25 °C into the dimeric {POM₂L₃} species; (b) splitting of the ¹⁸³W NMR lines initially overlapped at -127.9 ppm during the course of the kinetic; (c) graphical representation of the conversion of {POM₆L₉} at 25 °C as a function of time.

time. At the beginning (2 h), the spectrum contains three observable lines at -127.9, -143.0, and -147.0 ppm with intensity ratios 6:1:2. However, the -127.9 ppm line (with a relative intensity of 6 with respect to resonance -143 ppm) exhibits an asymmetric shape and splits into three equal components with increasing time (see Figure 8, panels a and b). Actually, the initial ¹⁸³W NMR spectrum of KLi₃₅-1a must be interpreted as a five lines spectrum with intensity ratios (2:2:2):1:2 because three of them overlap accidentally. Such a result appears to be fully consistent with the D_{3h} {POM₆L₉} arrangement observed in KLi₃₅-1a. As time increases, two simultaneous events are observed: (i) the continuous intensity decrease of intensity for the five resonances initially observed at ~-127.9, -143.0, and -147.0 ppm for the benefit of two growing signals at -114.7 and -140.0 ppm and (ii) the variation of the chemical shifts of the initial resonances at -127.9, -143.0, and -147.0 ppm, which leads to the splitting of the overlapped resonances at -127.9 ppm into three components (see Figure 8b). In summary, the ¹⁸³W NMR evolution can be reasonably interpreted as a five lines spectrum that converts into a 2:1 lines spectrum. After 88 h, only the 2:1 signals are present showing the complete conversion of the hexamodular anion **1a** into a new species. Among the three compounds **1**, **2** and **3** deriving from the {AsW₉O₃₃}-{Mo₂O₂S₂} system, only the {POM₂L₃} anion [(AsW₉O₃₃)₂(Mo₂O₂S₂)₃]¹²⁻ (**3**) with D_{3h} symmetry is consistent with the 2:1 observed signals. Further experiments confirm the attribution of these 2:1 resonances to **3** and the instability of **1** as lithium salt, which converts spontaneously into the dimeric species. The ¹⁸³W NMR spectrum of the pure lithium salts Li₁₂**3** and Li₃₆**1** (obtained through cationic resin exchange from Cs₉Li₃**3** and K_{3.5}Na_{32.5}**1a**, respectively) gave exactly the same 2:1 resonances at -114.9 and -140.0 ppm (see Figure 7b). From integration of the ¹⁸³W NMR lines, the fractions of {POM₆L₉} can be calculated, giving the kinetic plot shown in Figure 8c. Full understanding of the {POM₆L₉} behavior in solution needs further data, especially about the key role of the cation upon the stability of the hexameric scaffold.

Then, the conversion of KLi₃₅-**1** into **3** has been studied through ³⁹K NMR experiments, which were carried out in the same conditions as the previous ¹⁸³W NMR study ($T = 293$ K, 0.1 mol·L⁻¹ in KLi₃₅-**1**). The ³⁹K NMR spectra, recorded at 1 h intervals (Figure 9a) reveal a single broad resonance ($\Delta\nu_{1/2} = 3200$ Hz), initially observed at $\delta = -20.5$ ppm, which gradually shifts toward low frequencies and concomitantly sharpens as time increases (see Figure 9, panels b and c). After 63 h, the ³⁹K NMR single line is observed at -13.3 ppm with $\Delta\nu_{1/2} = 390$ Hz (see Figure 9, panels b and c). The ³⁹K NMR is well documented, especially in the field of biological systems and structures because of the significance of K⁺ ions.³⁰ The observed variation of the ³⁹K NMR parameters during the kinetic experiment features the change of the environment in the K⁺ coordination sphere. The initial broad resonance ($\Delta\nu_{1/2} = 3200$ Hz) observed at -20.5 ppm reflects a significant electrical field gradient (efg) around ³⁹K nuclei, with a reasonably long correlation time of the fluctuating efg. Such a situation is consistent with a fast exchange on the NMR time scale between coordinated potassium ions embedded within the cavity of the {POM₆L₉} ion and aqueous potassium. After 63 h, the ³⁹K NMR resonance exhibits a line width of 390 Hz at -13.3 ppm. In addition to the line width and chemical shift variations, the line area A_{obs} of the ³⁹K NMR signal increases continuously from 10000 a.u. to 32200 a.u. (see Figure 9d). The variations of the ³⁹K NMR parameters, i.e., line width, chemical shift, and signal amplitude, arise from a common phenomenon, which reflects the change of the ³⁹K environment during the course of the kinetic. Such a process is consistent with a net K⁺ release from a crypted situation in the cavity of the {POM₆L₉} anion (noted K_{crypt}⁺) to solvent as aqua ion (noted K_{aq}⁺). In the case of crypted potassium ion, ³⁹K is expected to experience a high relaxation rates because of a stronger efg and a longer correlation time due to the size of the cryptand.³¹ Furthermore, a screening effect at the crypted potassium nucleus should be due to the {POM₆L₉} shell. Conversely, aqueous potassium ions K(OH)₂⁺ retain a labile and nearly spherical environment featured by a narrower and high frequency shifted signal.³²

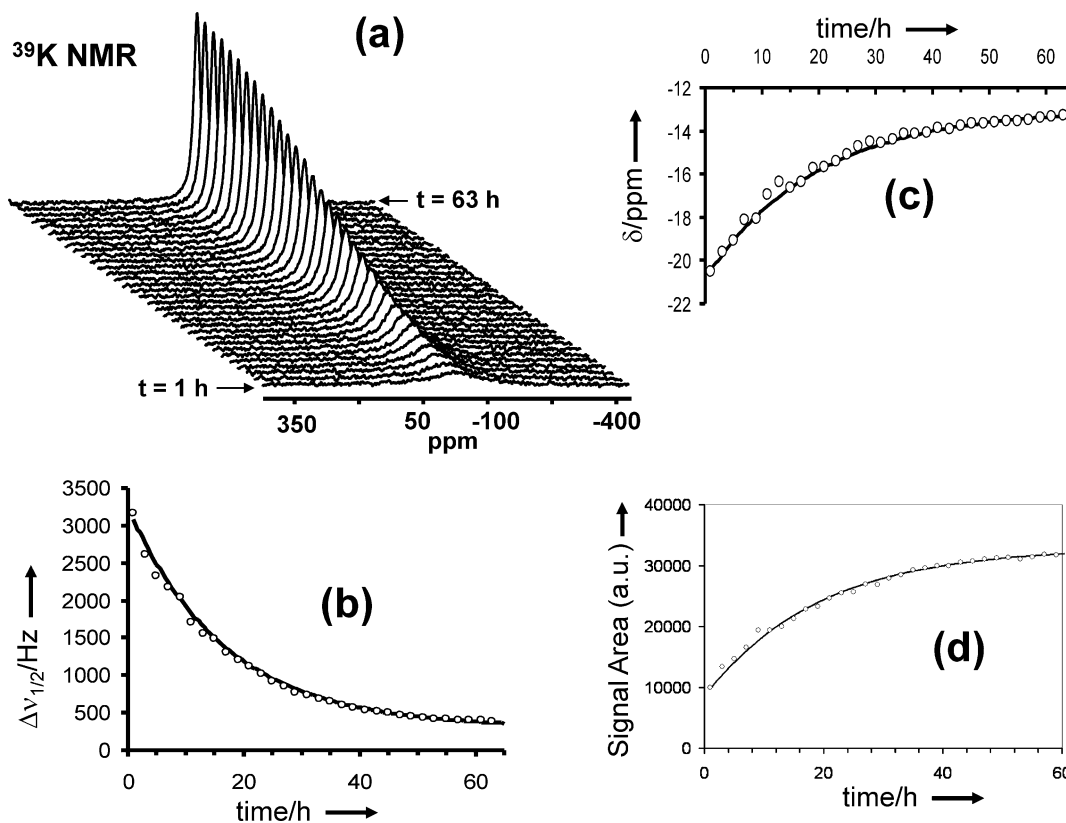


Figure 9. (a) Selected ^{39}K NMR spectra of $\text{KLi}_{35}\text{-1}$ as a function of time. Graphical representation of ^{39}K NMR parameters as a function of time: (b) line width, (c) chemical shift, and (d) line area.

The variation of the signal amplitude must be related to the extremely short relaxation time T_2 due to the reduced symmetry around the crypted K^+ ion and to the increase of the correlation time, which precludes any detection of the corresponding free induction decay in the conditions of the ^{39}K NMR experiment (spin-echo sequence). Such a statement is to some extent fulfilled by previous ^{39}K NMR investigations of some K-complexes.^{33,34} Due to severe line broadening, no relaxation data could be obtained from potassium cation trapped by crown-ether such as [dibenzo-18-crown-6] or cryptand-[222] molecules.^{33,35} Quantitative analysis (see below) of both ^{183}W and ^{39}K NMR kinetic experiments of $\text{KLi}_{35}\text{-1}$ seems to evidence two correlated events identified as the slow conversion of the $\{\text{POM}_6\text{L}_9\}$ anion **1a** into the $\{\text{POM}_6\text{L}_3\}$ species **3**, leading consequently to the net increase of K_{aq}^+ concentration. In addition, such a conversion process has to be coupled to the release of lithium cations toward the solvent because inner Li^+ has been structurally located in the initial $\text{KLi}_{35}\text{-1}$ compound. Besides, the increase of aqueous potassium ions concentration during the course of the kinetic experiment appears to be also at the origin of the ^{183}W chemical shifts. As shown in Figure 8b, three of them, initially overlapped at -127.9 ppm, gradually split with time into three components observed at -123.4 , -130.7 , and -132.0 ppm after about 60 h. To verify this assumption, ^{183}W NMR spectra of $\text{KLi}_{35}\text{-1}$ have been recorded with variable amounts of KCl. The NMR data were obtained at $T = 293$ K for $\text{K}^+/\{\text{POM}_6\text{L}_9\}$ ratios varying from 1 to 25 and revealed that the initial ^{183}W NMR spectra exhibit always five resonances with 2:1:2:2:2 intensity ratio, in agreement with a D_{3h} symmetry for the $\{\text{POM}_6\text{L}_9\}$ architecture. The D_3 staggered conformer corresponding to the **1b** arrangement was

never observed as frozen arrangement in solution probably because the fast exchange between the inner and outer potassium ions can lead to a dynamic averaged D_{3h} symmetry on the NMR time scale or to a D_{3h} relaxed arrangement similar to that observed in **1a**. At this step, nothing allows to discriminate both possible situations. Nevertheless, as surmised, the five ^{183}W NMR resonances of the $\{\text{POM}_6\text{L}_9\}$ scaffold appear to be significantly sensitive to the nature of the counter-cations (see Figure 10a), thus reflecting specific anion–cation interactions within the cavity. For example, the three high frequency 2W lines (initially overlapped at -127.9 ppm) exhibits similar behaviors that those observed during the kinetics presented in Figure 9, confirming that the observed evolution of the chemical shifts is due to successive and concomitant events listed as (i) the conversion of the $\{\text{POM}_6\text{L}_9\}$ into the dimeric species which constitutes the driving force of the process, (ii) the resulting potassium release, and (iii) the uptake of potassium ions by the unconverted $\{\text{POM}_6\text{L}_9\}$ self-assembly. In addition, the influence of the $\text{K}^+/\{\text{POM}_6\text{L}_9\}$ ratio upon the conversion rate has been studied. Whatever the $\text{K}^+/\{\text{POM}_6\text{L}_9\}$ ratios varying from 1 to 25, the five-line spectrum is invariably converted into a two-line spectrum but the initial rate constant of the process is significantly affected (see Figure 10b). As the potassium content increases from 1 to 25 equivalents, the initial rate constant decreases from about 0.07 to 0.02 h^{-1} , showing that potassium ions govern the kinetic stability of the $\{\text{POM}_6\text{L}_9\}$ scaffold.

Semiquantitative Analysis of Kinetic Experiments. The ^{183}W and ^{39}K NMR studies have produced a reliable set of structural and kinetic data about the behavior of the $\{\text{POM}_6\text{L}_9\}$ self-assembly in solution, which can be further

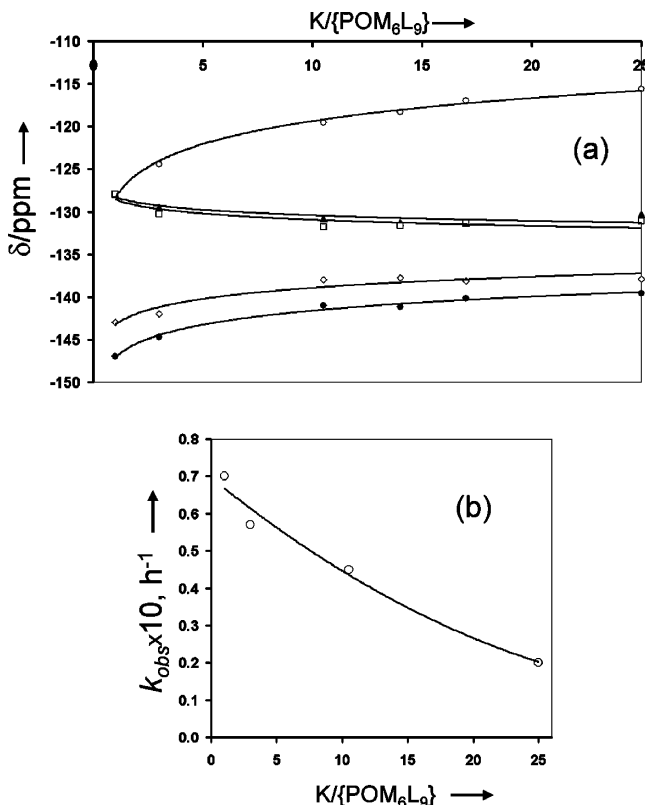
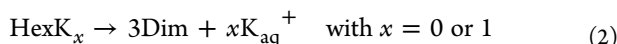


Figure 10. (a) Shifts of the ^{183}W NMR resonances for the $\text{KLi}_{35}\text{-1a}$ compound with increasing equivalent of KCl. (b) Graphical representation of the kinetic constant k_{obs} with increasing equivalent of KCl.

analyzed in a semiquantitative way. The analysis of the ^{39}K NMR parameters observed for $\text{KLi}_{35}\text{-1a}$ in solution (see Figure 9) seems to indicate that the single potassium ion is exchanging between the large cavity of the $\{\text{POM}_6\text{L}_9\}$ and the solution. Nonetheless, X-ray analysis of $\text{KLi}_{35}\text{-1a}$ did not allow locating any potassium ion, meaning that in the solid state, this ion is severely disordered with water molecules. This result, corroborated by the ^{183}W chemical shifts dependence (see Figure 10) indicates that the $\{\text{POM}_6\text{L}_9\}$ cluster has a higher affinity for potassium than for lithium ions. During the kinetic experiment, the hexameric scaffold should be distributed as two main species such as a potassium containing $\text{K}@\{\text{POM}_6\text{L}_9\}$ (abbreviated HexK, hereafter) and a potassium free species (abbreviated Hex), involved in the equilibrium expressed by eq 1. As the potassium exchange is found to process fast, we can assume that the distribution of the HexK and Hex species remains close to equilibrium during the overall kinetic process expressed by eq 2, where Dim corresponds to the dimeric association 3

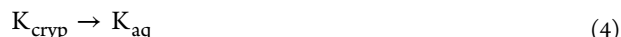


The main difficulty for modeling the ^{39}K and ^{183}W NMR data lies in the determination of the initial proportion of the species involved in eq 1. This difficulty can be tentatively solved from the ^{39}K NMR study. Seemingly, the variation of the ^{39}K NMR line area (shown in Figure 9d) means that crypted potassium ions $\text{K}_{\text{crypt}}^+$ produce an extremely broad signal that could not be detected and at the origin of signal loss. The lack of signal for trapped potassium cations has been already

reported with some organic cryptands.^{33,35} In such conditions, the normalized line area, noted A_N (expressed in arbitrary unit), can be expressed as function of the fraction of aqueous potassium (x_K) (given in eq 3)

$$A_N = \alpha/\beta x_{\text{HK}} + x_K \quad (3)$$

where α and β represent the observability factor of the crypted and aqueous potassium ions, respectively. The treatment of eq 3 in regard with the experimental ^{39}K NMR acquisition parameters is detailed in the Supporting Information section (see SI 2, Supporting Information). Such a treatment allows to estimate the initial conditions (at $t = 0$), which correspond to $x_K^0 = x_H^0 = 0.27$ and $x_{\text{HK}}^0 = 0.73$. Furthermore, the conditional equilibrium constant K_{eq} associated to eq 1 can be calculated from these values giving $K_{\text{eq}} = 10^{-2} \text{ mol}^{-1}\text{L}$. Then, the fraction of aqueous potassium over the kinetic experiment $x_K(t)$ can be calculated from the ^{39}K NMR parameters either line width, chemical shift or line area (see Table SI3, Supporting Information). The $x_K(t)$ calculations obtained from the three ^{39}K NMR parameters produce very close curves (See Figure SI3, Supporting Information), confirming that the variations of the ^{39}K NMR parameters are related to a common process: the net release of potassium ion expressed as eq 4. The $x_K(t)$ curves fit perfectly a first-order law



giving a kinetic constant $k_K = 0.052 \pm 0.02 \text{ h}^{-1}$ for eq 4 (see Figure SI4, Supporting Information). The fraction of the hexameric $\{\text{POM}_6\text{L}_9\}$ scaffold into the dimeric species $\{\text{POM}_2\text{L}_3\}$ can be easily calculated from the integrated ^{183}W NMR resonances (see Figure 8c). As surmised, the kinetic law according to eq 2 does not fit satisfactorily a first-order plot. The main reason is probably due to the dependence of the kinetic constant (noted k_{obs}) with the potassium content within the hexameric scaffold as has been previously evidenced (see Figure 10b). In other words, the involved species HexK and Hex convert into the dimeric species with their own reaction rate. The initial conversion rate agrees with $k_{\text{obs}} = 0.076 \text{ h}^{-1}$ while at the end of the process (after about 50 h), k_{obs} decreases until 0.054 h^{-1} . In consequence, we could approximate that k_{obs} varies continuously between these limit values. The simplest simulation considers a linear variation of k_{obs} between these two limit values, which provide calculated fractions of $\{\text{POM}_6\text{L}_9\}$ species in fair agreement with experimental values (see Figure 11). From the calculated K_{aq}^+ and $\{\text{POM}_6\text{L}_9\}$ fractions, the speciation of $\{\text{POM}_6\text{L}_9\}$ scaffold into the potassium-free and potassium-containing species (noted Hex and HexK, respectively) can be achieved using the equilibrium constant $K_{\text{eq}} = 10^{-2} \text{ mol}^{-1}\text{L}$ associated to eq 1. The calculated fractions x_H and x_{HK} are graphically shown in Figure 11. As the ratio between the proportion of Hex and HexK are at the origin of the ^{183}W NMR chemical shifts variation during the kinetic process (as shown in Figure 8b), it becomes also possible to calculate the fractions x_H and x_{HK} from the ^{183}W NMR chemical shifts. Among the five ^{183}W NMR lines, the high frequency resonance (δ_1) exhibits the strongest dependence toward the encapsulation of potassium ion ($\Delta\delta_1 \approx +5 \text{ ppm}$ from $t = 0$ to 60 h) and should be preferentially used to calculate the fraction x_H and x_{HK} . The initial and final proportions in Hex and HexK (0.27 and 0.73, respectively) allow obtaining the chemical shift δ_1 of these species ($\delta_1(\text{Hex}) = -140.0 \text{ ppm}$ and $\delta_1(\text{HexK}) = -123.4 \text{ ppm}$), then used to calculate x_H and x_{HK} as a function of time. These

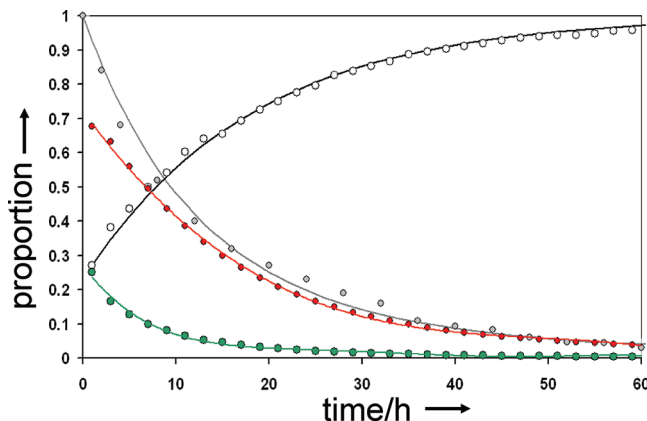


Figure 11. Graphical representation of fraction in aqueous potassium (black), total hexameric species (gray), HexK (red), and Hex (green). Dots = experimental, continuous lines = calculated.

results graphically shown in Figure 11 are in fair agreement with those previously calculated from kinetic and equilibrium constants. Overall results give a consistent link between the ^{39}K and ^{183}W NMR experiments and support the proposed kinetic model.

UV–Visible Experiments. The synthesis conditions of the clusters supported by the ^{39}K and ^{183}W NMR experiments presented previously indicate clearly the prominent templating role played by the alkali cations and the stabilizing influence of potassium and sodium toward the $\{\text{POM}_6\text{L}_9\}$ cage in aqueous solution. Consequently, it was decided to investigate the stability of the $\{\text{POM}_6\text{L}_9\}$ anion in diluted solution (about 10^{-4} M in $\text{KLi}_{35}\text{--1a}$) by using UV–vis spectroscopy. The electronic spectra of $\{\text{Mo}_2\text{O}_2\text{S}_2\}$ -containing polyoxotungstates are dominated by strong LMCT transitions $\text{E} \rightarrow \text{Mo}^{\text{V}}$ with $\text{E} = \text{O}, \text{S}$ observed in the visible region and are at the origin of red-brown color solutions.²⁵ The UV–vis spectrum of fresh aqueous solution of $\text{KLi}_{35}\text{--1a}$ exhibits two shoulders at 410 nm ($\epsilon = \sim 38\,000\text{ mol}^{-1}\cdot\text{L}\cdot\text{cm}^{-1}$) and 350 nm ($\epsilon = \sim 87\,500\text{ mol}^{-1}\cdot\text{L}\cdot\text{cm}^{-1}$) but solutions of $\text{KLi}_{35}\text{--1a}$ revealed unstable as indicated by a significant and rapid color change from red to yellow in about 20 min at $T = 25\text{ }^\circ\text{C}$ (see Figure S15, Supporting Information). The features of the resulting spectrum, supported by the resulting yellow solution are consistent with a complete dissociation of the scaffold complex into unidentified polyoxotungstate ions which absorb only in the UV domain (below 300 nm) and $\{\text{Mo}_2\text{O}_2\text{S}_2\}$ -based

cyclic oxothiomolybdates giving weak absorptions between 350 and 380 nm responsible for the yellow color solutions.³⁶ The variation of the molar absorption coefficient at 350 nm (ϵ_{350}) with time, graphically shown in Figure 12 reveals that in such diluted conditions, the kinetics of the dissociation process terminates after about 15–20 min in water while the conversion of the $\{\text{POM}_6\text{L}_9\}$ scaffold into the dimeric species, observed for concentrated solutions (about $10^{-1}\text{ mol}\cdot\text{L}^{-1}$) takes approximately about 80 h to be completed. Still here, despite the diluted conditions, the presence of potassium ions affects spectacularly the rate of the $\{\text{POM}_6\text{L}_9\}$ dissociation (see Figures 12a and 12b). The relative initial rates of dissociation (noted R), calculated from the variations of the molar extinction coefficient at 350 nm (ϵ_{350}) are shown in Figure 12b. The relative initial rates of dissociation vary dramatically from $R = 1$ to values close to zero for KCl concentration increasing from 0 to $2.5 \times 10^{-3}\text{ mol}\cdot\text{L}^{-1}$. For higher KCl concentrations, solutions did not lead to any significant change in their color or spectroscopic properties, indicating that dissociation of the $\{\text{POM}_6\text{L}_9\}$ scaffold appears quite canceled over the kinetic time scale. Such UV–vis experiments highlight the prominent templating ability of potassium cation, crucial to maintain the scaffold self-assembly.

DFT Calculations. We have applied the density functional theory (DFT) in the gas phase or with the COSMO (see Computational Details) to compute the geometries and energies of the dimer (3), tetramer (2) and hexamer (1a and 1b). Thanks to the good balance between accuracy and computational cost, the DFT has shown its ability to reproduce and explain experimental observations of diverse nature in the field of POMs.³⁷

Dimeric Arrangement, $\{\text{POM}_2\text{L}_3\}$ (Anion 3). For the simplest compound of the series we carried out two geometry optimizations: (i) within the gas-phase approximation (isolated molecule) and (ii) taking into account the solution effects with the COSMO.^{38,39} Both optimized geometries are very similar, indicating that 3 is rigid and is hardly affected by its environment, though the COSMO-optimized geometry agrees better with the experimental one, as expected. Especially the parameters listed in Table 1 show that considering the solvent effects makes the cluster more compact. Other geometrical parameters, such as interatomic distances of bonded atoms, are in perfect agreement with the X-ray structure. This behavior may be attributed to the stabilizing effect of the solution upon the high negative charge of -12 carried by this cluster. Since accounting for the external (solvent and counterions) effects

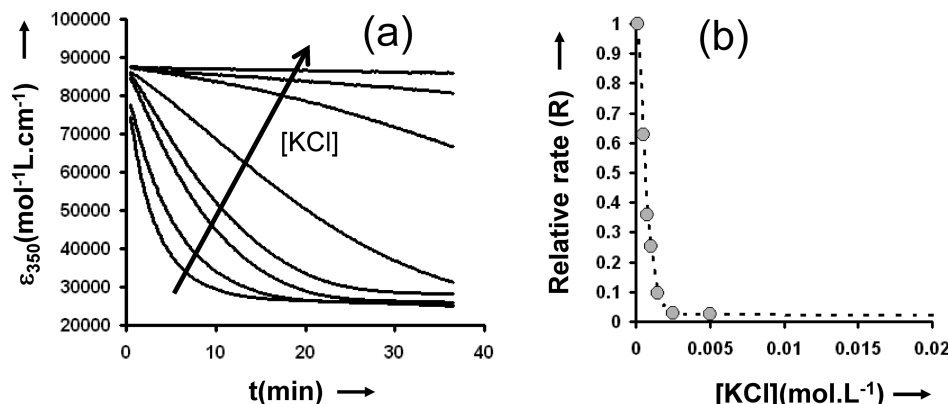


Figure 12. Effect of potassium cation upon the dissociation process of the $\{\text{POM}_6\text{L}_9\}$ scaffold in diluted conditions. (a) Variation of the molar extinction coefficient at 350 nm (ϵ_{350}) of $10^{-4}\text{ mol}\cdot\text{L}^{-1}$ aqueous solution in $\text{KLi}_{35}\text{--1a}$ vs time; (b) Variation of the relative dissociation constant (noted R) as a function of KCl concentration, varying from 10^{-4} to $5 \times 10^{-2}\text{ mol}\cdot\text{L}^{-1}$.

Table 1. Selected Interatomic Distances (in Å) Computed for {POM₂L₃} Arrangement (Anion 3)

	gas	water	X-ray
<i>d</i> (As···As)	8.617	8.306	8.332
<i>d</i> (Mo···Mo)	3.007	2.897	2.863
<i>d</i> (S···S)	4.01	3.741	3.595

suffices to reproduce the experimental structure, we can confirm that no cations are present inside the cavity.

Terminal oxygen atoms of the {Mo₂} linkers can, in principle, be oriented inward or outward the cluster cavity. The most stable configuration computed for 3 has three {Mo₂} groups pointing outward featuring solvent-stabilizing interactions and avoiding the internal region of high negative potential.

Tetrameric Arrangement, {POM₄L₆} (Anion 2). The larger size of the internal cavity of 2 increases the complexity of this system. It allows encapsulating cations, notably Rb⁺, and due to the larger separation between neighboring {Mo₂} linkers, the inward orientation of the Mo=O groups is energetically more affordable than in 3. If no Rb⁺ are present in the cavity, the negative potential inside pushes the Mo=O groups outward even for gas-phase calculations. The energies for the optimized structures (inward/outward) 6:0, 5:1, and 4:2 show a ~13 kcal·mol⁻¹ stabilization per additional outward Mo=O group. When the COSMO is introduced, the Mo=O···solvent interactions favor even more the outward orientation. So, the structure with outward {Mo₂O₂S₂} groups is the preferred one since it diminishes the internal destabilizing steric interactions (see Table 2). The same conclusion is achieved at a qualitative level upon inspection of the molecular electrostatic potential (MEP) shown in Figure 13.^{40,41} There is a major tendency to feature outer {Mo₂O₂S₂} groups due to the highly negative potential inside the cluster. Also, two minima have been identified from DFT calculations at the positions where Rb⁺ cations are found experimentally, i.e., at the center of the four faces of the {POM₄L₆} super tetrahedron.

Calculations reveal that 2 is more flexible than 3. The geometry optimization in gas phase without the internal Rb⁺ cations show that the As···As, Mo···Mo, and especially S···S distances are notably longer than the experimental ones (Table 2). This indicates that the high negative charge of 2 (-24) pushes the {Mo₂} linkers outward. The gas-phase optimized 6:0

Table 2. Selected Computed and X-ray Distances (in Å) for Anion 2

	gas	gas	gas
{POM ₄ L ₆ }	6:0 ^b	5:1 ^b	4:2 ^b
ΔE^a	0.0	-13.6	-26.3
<i>d</i> (As···As)	11.94	11.92	11.94
<i>d</i> (Mo···Mo)	3.11	3.11	3.11
<i>d</i> (S···S)	7.63	7.60	7.56
	gas	water	X-ray
2Rb ⁺ C {POM ₄ L ₆ }	5:1	5:1	5:1
<i>d</i> (As···As)	12.120	11.363	11.068
<i>d</i> (Mo···Mo)	3.052	2.909	2.85
<i>d</i> (S···S)	6.642	5.502	5.544
<i>d</i> (S···S)	7.179	5.793	5.544
<i>d</i> (Rb-O)	3.542	3.327	3.232

^aRelative energies of gas-phase and COSMO calculations are in kcal·mol⁻¹. ^bX:Y refers to the ratio of the {Mo₂O₂S₂} linkers with inward- and outward-oriented Mo=O bonds, respectively.

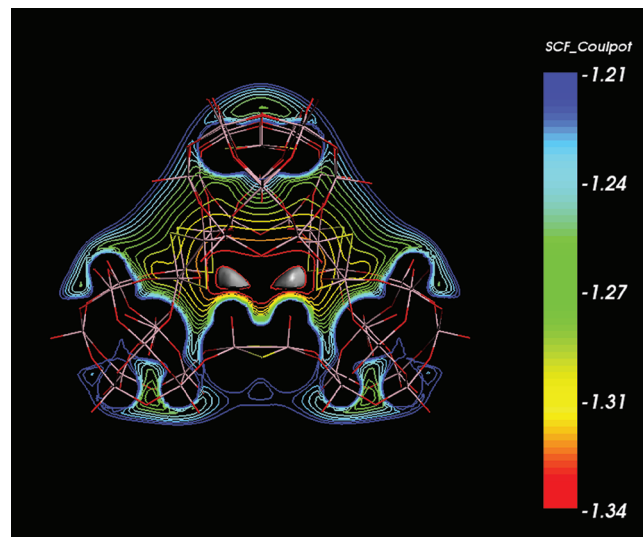


Figure 13. Molecular electrostatic potential plotted in a plane coinciding with the C₂ symmetry axis of 2. Superimposed there are the two potential minima, as gray isosurfaces, found at V = -1.34 au. The electrostatic potential is colored to represent more negative values (red) and less negative (or positive) values (blue). See text for details.

structure has *d*(S···S) = 7.63 Å. Inclusion of two Rb⁺ ions (with a concomitant reversal of one linker to give the 5:1 form) produces *d*(S···S) = 6.64–7.18 Å, which turns into 5.50–5.79 Å (close to the X-ray value, 5.54 Å) when the solution effects are accounted for. Therefore, Rb⁺ act as glue and the solvent does the rest. It can be also observed that the 5:1 structure (the experimental one) gets more compact upon addition of the solvent + counterions effects from the *d*(As···As) separation, which shortens from 12.12 to 11.36 Å (X-ray: 11.07 Å).

Hexameric Arrangement, {POM₆L₉} (Anion 1). Two conformations, labeled **1a** and **1b**, have been observed for the hexamer. There are two types of linkers: the horizontal ones, belonging to the same {POM₃L₃} basal unit (Figure 2a), and the vertical ones, or pillars, connecting {POM₃L₃} units. Structure **1a**, with D_{3h} point symmetry without internal counterions or waters, has been computed in two different ways:

- (i) A full geometry optimization. Both types of {Mo₂O₂S₂} linkers display a high degree of flexibility in this structure as shown in the evolution upon optimization of the eclipsed structure, **1a**. Starting approximately from the X-ray structure, with As–As and Mo–Mo distances shown in Figure S15, the cluster tends to open (as in a symmetric breathing mode) going toward an unrealistic form with very long {AsW₉O₃₃}–{AsW₉O₃₃} distances. The vertical {Mo₂O₂S₂} moieties also tend to go outward, both gas-phase and COSMO calculations leading to a similar result. Especially, the vertical pillars suffer important deformations to minimize the repulsion created by the high negative potential existing inside the cavity and the {AsW₉O₃₃} units. The presence of the solvent does not suffice to keep the cluster in a realistic compact form. Apparently, the role of the internal Na⁺ cations and water molecules in the {POM₆L₉} scaffold is fundamental, as in the tetrameric compound.
- (ii) A constrained optimization with the set of key distances shown in Figure S15 forced to remain constant at *d*(As···As)_v = 11.35 Å, *d*(As···As)_h = 10.72 Å, and

$d(\text{Mo}\cdots\text{Mo}) = 9.17 \text{ \AA}$. These restrictions keep the structure compact during the optimization, close to the experimental one. Now, we observe that the energy remains fairly constant but not reaching a minimum, indicating that the structure is quite flexible and some distortion is allowed without a great energy demand. We consider that the final geometry obtained (although not strictly a minimum) is acceptable for a qualitative analysis of some properties.

Structure **1** is larger than **2** and **3**, and it contains much free space in the cavity and in the windows that connect the inside with the outside of it. So, the free space inside allows Na^+ and water to be present in an ordered pattern that follows the potential energy minima of the cavity (see Figure 14). The potential

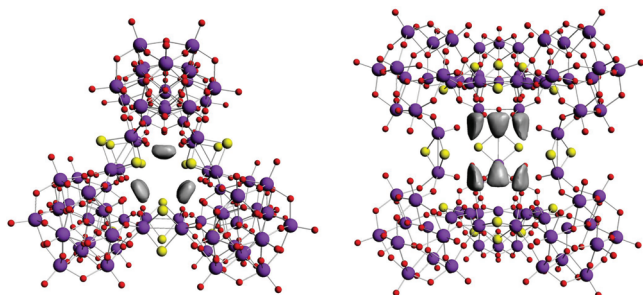


Figure 14. Electrostatic potential minima at $V = -1.76 \text{ au}$ (gray isosurface) found in structure **1a** (top and side views).

energy representation for **1a** shows the existence of six minima coinciding with the positions where Na atoms are found by X-ray. These cations, stabilized by the negative potential inside the highly charged (-36) cluster, can help the inward orientation of the $\text{Mo}=\text{O}$ units.

Structure **1b** has also been computed. From an initial staggered form (D_3 symmetry) with neither waters nor counterions, a free optimization leads to the eclipsed form, which turns to be the preferred one, at least in the absence of cations and waters. This result was not evident before doing the present calculations since the particular orientation of the $\{\text{AsW}_9\text{O}_{33}\}$ groups in the D_3 form might reduce their mutual electrostatic repulsion. We can thus tentatively propose that an energy balance exists between a destabilizing tension of the equatorial $\{\text{Mo}_2\text{O}_2\text{S}_2\}$ groups and an electrostatic stabilizing alternated conformation of the $\{\text{AsW}_9\text{O}_{33}\}$ units. The inclusion of Na^+ cations inside the eclipsed form has been tested. A partial geometry optimization without restrictions still shows a certain tendency of the structure to open, but much less than without cations. The six Na^+ atoms are attracted by the negative charges residing in the Keggin units thus helping the structure to remain compact. Finally, from X-ray data, three atoms were partially resolved in the equatorial region of the structure, in bridging positions between $\text{W}=\text{O}$ oxygens of two Keggin groups belonging to different triangular basal groups. DFT results confirm that counterions are attached in this fashion $\text{W}=\text{O}\cdots\text{M}^+\cdots\text{O}=\text{W}$, at $d(\text{M}^+-\text{O}) = 2.347 \text{ \AA}$, reproducing the positions encountered by X-ray (2.363 \AA).

SUMMARY AND CONCLUSION

We have shown that a carefully designed complementary system based on the trivacant $\{\text{AsW}_9\text{O}_{33}\}^{9-}$ POM unit and the $\{\text{Mo}_2\text{O}_2\text{S}_2\}^{2+}$ linker can be combined to build supramolecular

structures in self-assembly processes restricted only to the metal–ligand coordination. Depending on the nature and concentration of the alkali cations, hexamodular scaffold $\{\text{POM}_6\text{L}_9\}$, tetramodular $\{\text{POM}_4\text{L}_6\}$, or dimodular $\{\text{POM}_2\text{L}_3\}$ assemblies are formed and isolated. The large hexameric scaffold has been isolated as two distinct conformations, i.e., eclipsed and staggered, showing rare flexibility properties for polyoxometalates yet described as rigid oxo close-packing arrangements. Structural analysis has revealed that conformational design of the inorganic scaffold is mainly governed by the nature of the cations (Na^+ or K^+) included in the inner-phase of the molecular host. Solution studies, carried out by ^{183}W and ^{39}K NMR and UV-vis disclose that the self-assembly is highly versatile and sensitive to the nature of alkali cations, highlighting their crucial role upon the processes. The important templating role that cations can play in the formation of supramolecular assemblies lies in the orientation of the coordinated $\{\text{Mo}_2\text{O}_2\text{S}_2\}$ linkers. Inward $\{\text{Mo}=\text{O}\}$ groups lead to the hexameric scaffold or tetrahedral arrangement with associated embedded cations while outward $\{\text{Mo}=\text{O}\}$ groups are observed in the simplest dimeric assembly. Na^+ and K^+ cations (and Li^+ in a less extent) favor the formation of the largest hexameric structure, forming well-defined inner cationic aquo clusters while Rb^+ and Cs^+ give rise to tetrahedral $\{\text{POM}_4\text{L}_6\}$ arrangements. The design strategy will hopefully guide the design and synthesis of new clusters based on the templating role of a variety cations such as divalent alkali-earth or organic cations. Given the possibility of creating clusters with well-defined cavities, this seems a desirable goal in light of the rich chemistry anticipated in the inner-phase of these molecular hosts. We also anticipate that these flexible, kinetically and thermodynamically stable, metrically well-defined clusters will find a use as component in nanotechnological applications.

ASSOCIATED CONTENT

S Supporting Information

Physical methods (NMR, X-ray crystallography, and computational details) and syntheses of the compounds (SI, 1). Determination of the initial conditions from ^{39}K NMR line area (SI, 2). Calculation of the fraction of aqueous potassium versus time (SI, 3). First-order law for the aqueous potassium formation (SI, 4). UV-vis of $\text{KLi}_{35}\text{-1a}$ in aqueous solution (SI, 5). Geometry evolution of **1a** during DFT optimization (SI, 6). Additional references (SI, 7). This material is available free of charge via the Internet at <http://pubs.acs.org>.

AUTHOR INFORMATION

Corresponding Author

cadot@chimie.uvsq.fr

ACKNOWLEDGMENTS

E.C. gratefully acknowledges the Centre National de la Recherche Scientifique (CNRS) and the Ministère de l'Enseignement Supérieur et de la Recherche (MESR) for their financial support. J.M.P. thanks the MICINN of Spain (CTQ2008-06549-C02-01/BQU) and the Generalitat de Catalunya (2009SGR-00462 and XRQTC) for financial support. X.L. thanks the Ramón y Cajal program (RYC-2008-02493).

REFERENCES

- (a) Fujita, M.; Umemoto, K.; Yoshizawa, M.; Fujita, N.; Kusukawa, T.; Biradha, K. *Chem. Commun.* **2001**, 509. (b) Fujita, et al. *Angew. Chem., Int. Ed.* **2003**, 42, 3909. (c) Caulder, D. L.; Brückner, C;

- Powers, R. E.; König, S.; Parac, T. N.; Leary, J. A.; Raymond, K. *J. Am. Chem. Soc.* **2001**, *123*, 8923–8938.
- (2) (a) Yaghi, O. M.; O'Keeffe, M.; Ockwig, N. W.; Chae, H. K.; Eddaoudi, M.; Kim, J. *Nature* **2003**, *423*, 705. (b) Cheetham, A. K.; Rao, C. N. R. *Science* **2007**, *318*, 58. (c) Ferey, G. *Chem. Soc. Rev.* **2008**, *37*, 191.
- (3) (a) Conn, M. M.; Rebek, J. Jr. *Chem. Rev.* **1997**, *97*, 1647. (b) Sauvage, J. P., Dietrich-Buchecker, C., Eds.; *Molecular Catenanes, Rotaxanes and Knots: a journey through the world of Molecular Topology*; Wiley-VCH: Weinheim, Germany, 1999. (c) Loeb, S. J. *Chem. Commun.* **2005**, *1511*. (d) Leininger, S.; Olenyuk, B.; Stang, P. *Chem. Rev.* **2000**, *85*.
- (4) (a) Fiedler, D.; Bergman, R. G.; Raymond, K. N. *Angew. Chem., Int. Ed.* **2004**, *43*, 6748. (b) Yoshizawa, M.; Tamura, M. *Science* **2006**, *321*, 251.
- (5) (a) Hof, F.; Craig, S. L.; Nuckolls, C.; Rebek, J. Jr. *Angew. Chem., Int. Ed.* **2002**, *41*, 1488. (b) Rebek, J. Jr. *Angew. Chem., Int. Ed.* **2005**, *44*, 2068.
- (6) Férey, G.; Serre, C.; Devic, T.; Maurin, G.; Jobic, H.; Llewellyn, P. L.; De Weireld, G.; Vimont, A.; Daturi, M.; Chang, J.-S. *Chem. Soc. Rev.* **2011**, *40*, 550.
- (7) McKinlay, A. C.; Morris, R. E.; Horcajada, P.; Férey, G.; Gref, R.; Couvreur, P.; Serre, C. *Angew. Chem., Int. Ed.* **2010**, *49*, 6260.
- (8) (a) Bertaina, S.; Gambarelli, S.; Mitra, T.; Tsukerblat, B.; Müller, A.; Barbara, B. *Nature* **2008**, *453*, 203. (b) Winpenny, R. E. P. *Angew. Chem., Int. Ed.* **2008**, *47*, 7992.
- (9) (a) Müller, A. *Nature* **2007**, *447*, 1035. (b) Yan, J.; Gao, J.; Long, D.-L.; Miras, H. N.; Cronin, L. *J. Am. Chem. Soc.* **2010**, *132*, 11410. (c) Wassermann, K.; Dickman, M. H.; Pope, M. T. *Angew. Chem., Int. Ed.* **1997**, *36*, 1445. (d) Müller, A.; Krickemeyer, E.; Meyer, J.; Bögge, H.; Peters, F.; Plass, W.; Diemann, E.; Dillingen, S.; Nonnenbruch, F.; Randerath, M.; Menke, C. *Angew. Chem., Int. Ed.* **1995**, *34*, 2122. (e) Müller, A.; Krickemeyer, E.; Bögge, H.; Schimidtmann, M.; Peters, F. *Angew. Chem., Int. Ed.* **1998**, *37*, 3359. (f) Special Issue on Polyoxometalates. *Chem. Rev.* **1998**, *98*, 1–390. (j) Hill, C. L. *J. Mol. Catal. A* **2007**, *262*, 1.
- (10) (a) Dolbecq, A.; Dumas, E.; Mayer, C. R.; Mialane, P. *Chem. Rev.* **2010**, *110*, 6009. (b) Long, D.-L.; Tsunashima, R.; Cronin, L. *Angew. Chem., Int. Ed.* **2010**, *49*, 1736. (c) Long, D.-L.; Burkholder, E.; Cronin, L. *Chem. Soc. Rev.* **2007**, *36*, 105. (d) Ettedgui, J.; Diskin-Posner, Y.; Weiner, L.; Neumann, R. *J. Am. Chem. Soc.* **2011**, *133*, 188.
- (11) (a) Lehmann, J.; Gaita-Arino, A.; Coronado, E.; Loss, D. *J. Mater. Chem.* **2009**, *19*, 1672. (b) Charron, G.; Giusti, A.; Mazerat, S.; Mialane, P.; Gloter, A.; Miserque, F.; Keita, B.; Nadjo, L.; Filoromo, A.; Riviere, E.; Wernsdorfer, W.; Huc, V.; Bourgoin, J.-P.; Mallah, T. *Nanoscale* **2010**, *2*, 139.
- (12) (a) Newton, G. N.; Yamashita, S.; Hasumi, K.; Matsuno, J.; Yoshida, N.; Nihei, M.; Shiga, T.; Nakano, M.; Nojiri, H.; Wernsdorfer, W.; Oshio, H. *Angew. Chem., Int. Ed.* **2011**, *50*, 5715. (b) Al Damen, M. A.; Cardona-Serra, S.; Clemente-Juan, J. M.; Coronado, E.; Gaita-Arino, A.; Martí-Gastaldo, C.; Luis, F.; Montero, O. *Inorg. Chem.* **2009**, *48*, 3467. (c) Ritchie, C.; Ferguson, A.; Nojiri, H.; Miras, H. N.; Song, Y.-F.; Long, D.-L.; Burkholder, E.; Murrie, M.; Koegerler, P.; Brechin, E. K.; Cronin, L. *Angew. Chem., Int. Ed.* **2008**, *47*, 5609. (d) AlDamen, M. A.; Clemente-Juan, J. M.; Coronado, E.; Martí-Gastaldo, C.; Gaita-Arino, A. *J. Am. Chem. Soc.* **2008**, *130*, 8874. (e) Compain, J. D.; Mialane, P.; Dolbecq, A.; Mbomekalle, I. M.; Marrot, J.; Sécheresse, F.; Riviere, E.; Rogez, G.; Wernsdorfer, W. *Angew. Chem., Int. Ed.* **2009**, *48*, 3077.
- (13) (a) Weiner, H.; Finke, R. G. *J. Am. Chem. Soc.* **1999**, *121*, 9831. (b) Maksimchuk, N. V.; Timofeeva, M. N.; Melgunov, M. S.; Shmakov, A. N.; Chesalov, Y. A.; Dybtsev, D. N.; Fedin, V. P.; Kholdeeva, O. A. *J. Catal.* **2008**, *257*, 315. (c) Kikukawa, Y.; Yamaguchi, K.; Mizuno, N. *Angew. Chem., Int. Ed.* **2010**, *49*, 6096. (d) Okuhara, T.; Mizuno, N.; Misono, M. *Appl. Catal., A* **2001**, *222*, 63.
- (14) (a) Cooper, G. J. T.; Cronin, L. *J. Am. Chem. Soc.* **2009**, *131*, 8368. (b) Kawasaki, N.; Wang, H.; Nakanishi, R.; Hamanaka, S.; Kitaura, R.; Shinohara, H.; Yokoyama, T.; Yoshikawa, H.; Awaga, K. *Angew. Chem., Int. Ed.* **2011**, *50*, 3471.
- (15) (a) Gyu-Shik Kim, G.-S.; H. Zeng, H.; VanDerveer, D.; Hill, C. L. *Angew. Chem., Int. Ed.* **1999**, *38*, 3205. (b) Kortz, U.; Hussain, F.; Reicke, M. *Angew. Chem., Int. Ed.* **2005**, *44*, 3773.
- (16) (a) Rousseau, G.; Oms, O.; Dolbecq, A.; Marrot, J.; Mialane, P. *Inorg. Chem.* **2011**, *50*, 7376. (b) Godin, B.; Chen, Y. G.; Vaissermann, J.; Ruhlmann, L.; Verdaguer, M.; Gouzerh, P. *Angew. Chem., Int. Ed.* **2005**, *44*, 3072.
- (17) Fang, X.; Kogerler, P. *Angew. Chem., Int. Ed.* **2008**, *47*, 8123.
- (18) Antonio, M. R.; Nyman, M.; Anderson, T. M. *Angew. Chem., Int. Ed.* **2009**, *48*, 6136.
- (19) Miró, P.; Pierrefixe, S.; Gicquel, M.; Bo, C. *J. Am. Chem. Soc.* **2010**, *132*, 17787.
- (20) Akutagawa, T.; Daigoro Endo, D.; Noro, S.-I.; Cronin, L.; Nakamura, T. *Coord. Chem. Rev.* **2007**, *251*, 2547.
- (21) (a) Duval, S.; Pilette, M.-A.; Simonnet, C.; Marrot, J.; Sokolov, M. N.; Cadot, E. *Chem.—Eur. J.* **2008**, *14*, 3457–3466. (b) N. Leclerc-Laronze, N.; Marrot, J.; Thouvenot, R.; Cadot, E. *Angew. Chem., Int. Ed.* **2009**, *48*, 4986–4989.
- (22) (a) Cadot, E.; Sécheresse, F. *Chem. Commun.* **2002**, 2189. (b) Lemmonier, J. F.; Duval, S.; Floquet, S.; Cadot, E. *Isr. J. Chem.* **2011**, *51*, 290.
- (23) (a) Cadot, E.; Pilette, M.-A.; Marrot, M.; Sécheresse, F. *Angew. Chem., Int. Ed.* **2003**, *42*, 2173. (b) Pilette, M.-A.; Marrot, J.; Sécheresse, F.; Cadot, E. *Inorg. Chim. Acta* **2010**, *363*, 4253.
- (24) Tourne, C.; Tourne, G. *C. R. Acad. Sci. Paris* **1975**, *281 C*, 933.
- (25) Marrot, J.; Pilette, M. A.; Sécheresse, F.; Cadot, E. *Inorg. Chem.* **2003**, *42*, 3609.
- (26) (a) Kortz, U.; Savelieff, M. G.; Bassil, B. S.; Dickman, M. *Angew. Chem., Int. Ed.* **2001**, *40*, 3384. (b) Jeannin, Y.; Martin-Frère, J. *J. Am. Chem. Soc.* **1981**, *103*, 1664.
- (27) (a) Dolbecq, A.; du Peloux, C.; Auberty, A.-L.; Mason, S. A.; Barboux, P.; Marrot, J.; Cadot, E.; Sécheresse, F. *Chem.—Eur. J.* **2002**, *8*, 349. (b) Greenwood, N. N.; Earnshaw, A. *Chemistry of the Elements*; Pergamon: New York, 1984.
- (28) (a) Béreau, V.; Cadot, E.; Bögge, H.; Müller, A. *Inorg. Chem.* **1999**, *38*, 5803. (b) Pilette, M.-A.; Floquet, S.; Marrot, J.; Cadot, E. *Eur. J. Inorg. Chem.* **2011**, 3523.
- (29) Chen, Y.-G.; Gong, J.; Qu, L.-Y. *Coord. Chem. Rev.* **2004**, *248*, 245–260.
- (30) (a) Frausto da Silva, J. J. R.; Williams, R. J. P. *The Biological Chemistry of the Elements*; Oxford University Press: Oxford, UK, 1991. (b) Lippard, S. J.; Berg, J. M. *Principles of Bioinorganic Chemistry*; University Science Books: Mill Valley, CA, 1994. (c) Page, M. J.; Di Cera, E. *Physiol. Rev.* **2006**, *86*, 1049.
- (31) (a) Emsley, J.; Feeney, J.; Sutcliffe, H. *High-resolution NMR Spectroscopy*; Pergamon Press: Oxford, U.K., 1966.
- (32) (a) Lindman, B.; Forsén. In *NMR and the Periodic Table*; Harris, S., Mann, k. R., Eds.; Academic Press: New York, 1978; p 129. (b) B. E. Sahm, W.; Schwenk, A. Z. *Naturforsch., A* **1974**, *29A*, 1754.
- (33) Shporer, M.; Luz, Z. *J. Am. Chem. Soc.* **1975**, *97*, 665.
- (34) (a) Sokól, M.; Grobelny, J.; Jedliński, Z. *J. Magn. Reson. Chem.* **1990**, *28*, 934. (b) Sokól, M.; Grobelny, J.; Grobelny, Z.; Stolarzewicz, A. *J. Phys. Chem.* **1993**, *97*, 763.
- (35) Sokól, M.; Grobelny, J.; Grobelny, Z.; Stolarzewicz, A. *Spectrochim. Acta* **1991**, *47A* (11), 1547.
- (36) Lemonnier, J.-F.; Floquet, S.; Marrot, J.; Cadot, E. *Eur. J. Inorg. Chem.* **2009**, *5057*–*5065*.
- (37) (a) Poblet, J. M.; López, X.; Bo, C. *Chem. Soc. Rev.* **2003**, *32*, 297. (b) López, X.; Miró, P.; Carbó, J. J.; Rodríguez-Fortea, A.; Bo, C.; Poblet, J. M. *Theor. Chem. Acc.* **2011**, *128*, 393.
- (38) This is the continuum method that introduces, in a simple though satisfactorily manner,¹ the effects of the solvent and the necessary counterions surrounding the solute, each accounting for approximately 50% of its total stabilization.
- (39) Miró, P.; Poblet, J. M.; Bonet-Ávalos, J.; Bo, C. *Can. J. Chem.* **2009**, *87*, 1296.

(40) The MEP is a useful property that helps explaining phenomena with an electrostatic origin. MEPs allow identifying nucleophilic and electrophilic regions of a molecule. Thus one can predict, for example, the positions where cations are attracted to or whether two substituents attract or repel to each other.

(41) López, X.; Bo, C.; Poblet, J. M. *J. Am. Chem. Soc.* **2002**, *124*, 12574.